NANO LETTERS
Cite This: Nano Lett. 2018, 18, 4861−4865
Letter
pubs.acs.org/NanoLett

# Ballistic One-Dimensional Holes with Strong *g*-Factor Anisotropy in Germanium

R. Mizokuchi,[†] R. Maurand,[†] F. Vigneau,[†] M. Myronov,[*,‡] and S. De Franceschi[*,†]

[†]Université Grenoble Alpes & CEA, INAC-PHELIQS, F-38000 Grenoble, France
[‡]Department of Physics, University of Warwick, Coventry CV4 7AL, United Kingdom

Supporting Information

**ABSTRACT:** We report experimental evidence of ballistic hole transport in one-dimensional quantum wires gate-defined in a strained SiGe/Ge/SiGe quantum well. At zero magnetic field, we observe conductance plateaus at integer multiples of $2e^2/h$. At finite magnetic field, the splitting of these plateaus by Zeeman effect reveals largely anisotropic *g*-factors with absolute values below 1 in the quantum-well plane, and exceeding 10 out-of-plane. This *g*-factor anisotropy is consistent with a heavy-hole character of the propagating valence-band states, which is in line with a predominant confinement in the growth direction. Remarkably, we observe quantized ballistic conductance in device channels up to 600 nm long. These findings mark an important step toward the realization of novel devices for applications in quantum spintronics.

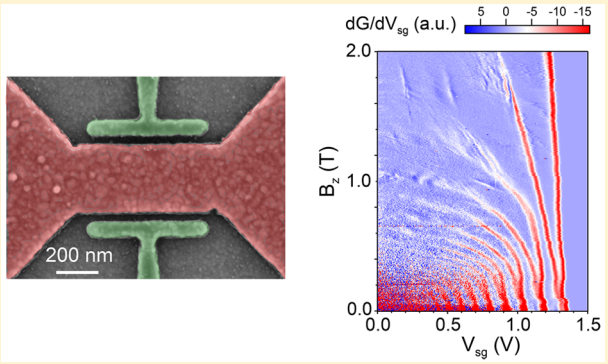


**KEYWORDS:** *Ballistic transport, holes, spintronics, germanium, g-factor, nanoelectronics*

Quantum spintronics is an active research field aiming at the development of semiconductor quantum devices with spin-based functionality.[1] This field is witnessing an increasing interest in exploiting the spin degree of freedom of hole spin states, which can present a strong spin−orbit (SO) coupling, enabling electric-field driven spin manipulation[2,3] and a reduced hyperfine interaction, favoring spin coherence.[4−6]

Efficient electric-dipole spin resonance was recently demonstrated for hole spins confined in silicon quantum dots.[7,8] Even faster manipulation should be possible in germanium, where holes have stronger SO coupling.[9] Germanium is also known to form low-resistive contacts to metals, owing to a Fermi-level pinning close to the germanium valence band. This property can lead to interesting additional opportunities, such as the realization of hybrid superconductor-semiconductor devices[10] (e.g., Josephson field-effect transistors,[11] gatemons,[12,13] and topological superconducting qubits based on Majorana Fermions,[14,15] for which the concomitant presence of strong SO coupling would play a key role).

Experimental realizations of Ge-based nanoelectronic devices have so-far relied primarily on bottom-up nanostructures: Ge/Si core/shell nanowires (NWs),[16−19] SiGe self-assembled quantum dots,[20,21] and Ge hut NWs.[22] Following recent progress in SiGe epitaxy, SiGe/Ge/SiGe quantum-well heterostructures embedding a high-mobility two-dimensional hole gas have become available,[23−25] providing a new attractive option for the realization of quantum nanoelectronic devices.[26−28]

Here we report the fabrication and low-temperature study of devices comprising a gate-tunable, one-dimensional (1D) hole channel with a gate-defined length varying between 100 and 900 nm. We reveal the ballistic 1D nature of hole transport through measurements of conductance quantization. By measuring the Zeeman splitting of the conductance plateaus in a magnetic field, $\vec{B}$, applied along different directions, we find a strong *g*-factor anisotropy consistent with a dominant heavy-hole (HH) character of the 1D subbands.

The devices were fabricated from a nominally undoped heterostructure consisting of a pseudomorphically strained, 22 nm thick Ge quantum well (QW) confined by $Si_{0.2}Ge_{0.8}$ barriers, that is, a relaxed $Si_{0.2}Ge_{0.8}$ buffer layer below, and a 72 nm thick $Si_{0.2}Ge_{0.8}$ layer above, capped by 2 nm of low-temperature-grown Si.[29] The heterostructure was grown by reduced pressure chemical vapor deposition on a Si(001) wafer (see ref 30 and details therein).

At low temperature, the Ge QW is carrier free, and hence insulating, due to the intentional absence of doping. A two-dimensional hole gas with a mobility of $1.7 \times 10^5$ cm$^2$/(V s) and a hole density of $\sim 10^{11}$ cm$^{-2}$ can be electrostatically induced by means of a negatively biased top gate electrode (for more details see Supporting Information).

**Received:** April 11, 2018
**Revised:** June 29, 2018
**Published:** July 11, 2018






DOI: 10.1021/acs.nanolett.8b01457
Nano Lett. 2018, 18, 4861−4865

The device layout consists of a large (tens of microns wide) mesa structure defined by optical lithography and reactive ion etching with $Cl_2$ gas. The dry etching process is calibrated to remove both the SiGe overlayer and the Ge quantum well.[31] Two platinum contact pads to be used as source and drain electrodes are fabricated on opposite sides of the mesa. Platinum deposition is carried out after dry-etch removal of the SiGe overlayer followed by a two-step surface cleaning process to eliminate the native oxide (wet HF etching followed by Ar plasma bombardment in the e-beam evaporator). We obtain contact resistances of the order of few kΩ. An $Al_2O_3$ 30 nm thick gate oxide layer is deposited by atomic layer deposition at 250 C°. Ti/Au top-gate electrodes are finally defined using e-beam lithography and e-beam metal deposition: a central gate extending over the mesa is designed to induce the accumulation of a conducting hole channel between the source to the drain contact; two side gates, to be operated in depletion mode, create a tunable 1D constriction in the channel oriented along the [100] direction. We have varied the geometry of the side gates in order to explore gate-defined 1D hole wires with different lengths. Here we present experimental data for two devices, one with a short (∼100 nm) and one with a long (∼600 nm) constriction (see Figure 1a,b, respectively).

All magnetotransport measurements were done at 270 mK in a $^3$He cryostat equipped with a superconducting magnet. Figure 1c shows a data set for a device, labeled D1, nominally identical to the one shown in Figure 1a. The differential conductance, $G$, measured at dc source-drain bias voltage $V_{ds} = 0$, is plotted as a function of $V_{sg}$ for magnetic fields, $\vec{B}$, perpendicular to the QW plane and varying from 0 to 0.5 T. In our experiment, $G$ was directly measured using standard lock-in detection with a bias-voltage modulation $\delta V_{sd} = 10\ \mu$V at 36.666 Hz. In addition, $G$ was numerically corrected to remove the contribution from all series resistances (∼20 kΩ), that is, the resistances of the measurement circuit, the source and drain contacts, and the two-dimensional hole gas.

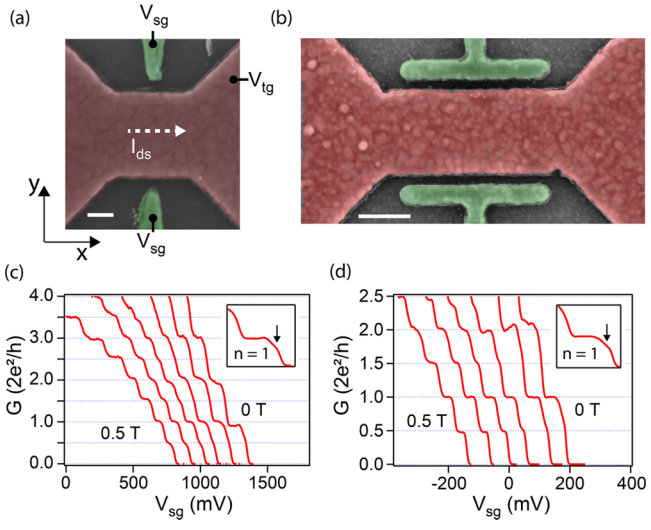


**Figure 1.** (a,b) False color scanning electron micrographs of representative devices. Scale bars: 100 nm (a) and 200 nm (b). Gate voltages $V_{tg} < 0$ and $V_{sg} > 0$ are applied to the channel gate (colorized in red) and the two side gates (colorized in green), respectively. Current $I_{ds}$ flows in Ge QW under the channel gate along the $x$-direction. To enable that, the channel gate extends of all the way to the source/drain contact pads, which are located about 15 $\mu$m away from nanowire constriction, that is, outside of the view field in (a,b). (c,d) Measurements of zero-bias conductance $G$ as a function of $V_{sg}$ at different perpendicular magnetic fields, $B_z$, from 0 to 0.5 T (step: 0.1 T). Data in (c) ((d)) refer to device D1 (D2), which is nominally identical to the one shown in (a) ((b)). In both cases, we observe clear conductance quantization and the lifting of spin degeneracy at finite field. Conductance has been rescaled to remove the contribution of a series resistance $R_S$ slightly varying with $B_z$ between 22 and 24 kΩ. The different traces are laterally offset for clarity. Insets: Zoom-in of the 0.7 anomaly (indicated by an arrow) at zero magnetic field.

$G$ exhibits clear quantized plateaus in steps of $2e^2/h$, where $e$ is the electron charge and $h$ is the Plank constant. This finding is consistent with the results of a recently published independent work carried out on a similar SiGe heterostructure.[26] Applying an out-of-plane magnetic field lifts the spin degeneracy of the 1D subbands, resulting in plateaus at multiples of $e^2/h$. These plateaus underpin the formation of spin-polarized subbands. They emerge at relatively small magnetic fields, of the order of a few hundred mT, denoting a large out-of-plane $g$-factor as expected in the case of a predominant HH character.

We measured several devices with side-gate lengths, $L_g$, ranging from 100 nm (as in Figure 1 a) to 900 nm. The $G(V_{sg})$ measurements shown in Figure 1d were taken on a device with $L_g \approx 600$ nm, labeled as D2 and nominally identical to the one shown in Figure 1b. Remarkably, these measurements demonstrate that clear conductance quantization can be observed also in relatively long channels largely exceeding 100 nm. Increasing the channel length should result in an appreciable sharpening of the conductance steps, reflecting a reduced probability of tunneling across the electrostatically induced potential barrier.[32] In our experiment, however, this effect is barely visible because the conductance step width is dominated by the thermal broadening of the Fermi distribution function in the leads.

We note that a shoulder at $G \sim 0.7 \times 2e^2/h$ is visible in the $B = 0$ traces of both Figure 1c,d. This feature, which is highlighted in the respective insets, corresponds to the so-called 0.7 anomaly. Discovered and widely studied in quantum point contacts defined in high-mobility two-dimensional electron systems[33−38] and more recently observed also in semiconductor nanowires,[39,40] the interpretation of this phenomenon remains somewhat debated.[41−45]

To further confirm the 1D nature of the observed conductance quantization, we present in Figure 2a−c waterfall plots of the nonlinear $G(V_{ds})$ at three different perpendicular magnetic fields ($B = 0$, 0.3, and 0.5 T, respectively) for device D1. Clear bunching of the $G(V_{ds})$ is observed around $V_{ds} = 0$ for gate voltages corresponding to the quantized conductance plateaus of Figure 1c. With magnetic field applied, the first plateau at $G = e^2/h$ begins to appear at $B = 0.3$ T and is fully formed at $B = 0.5$ T. At $B = 0$, a zero-bias $dI/dV$ peak can seen in correspondence of the 0.7 structure, which is in line with previous observations.[36]

The well-resolved spin splitting of the 1D subbands enables a quantitative study of the hole $g$-factors. To investigate the $g$-factor anisotropy, we applied $\vec{B}$ not only along the $z$-axis, perpendicular to the substrate plane, but also along the in-plane directions $x$ and $y$, indicated in Figure 1a. To change the $\vec{B}$ direction, the sample had to be warmed up, rotated, and cooled down multiple times. Thermal cycling did not modify significantly the device behavior, except for the value of threshold voltage on the channel gate for the activation of hole



DOI: 10.1021/acs.nanolett.8b01457
Nano Lett. 2018, 18, 4861−4865

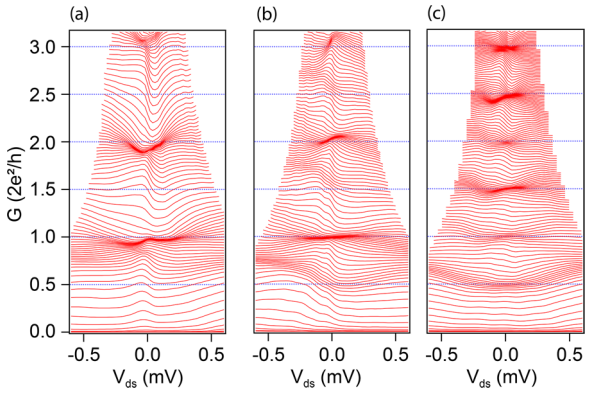


**Figure 2.** Waterfall plots of differential conductance, $G$, as a function of source-drain bias, $V_{ds}$, at different values of side-gate voltage $V_{sg}$ (gate step: 5 mV). The three plots were taken on device D1 at different out-of-plane magnetic fields: (a) 0 T, (b) 0.3 T, and (c) 0.5 T. The spanned $V_{ds}$ range varies with $V_{sg}$, and hence with $G$. This follows from the procedure used to take into account the effect of the series resistance, $R_S$. In this procedure, we assumed $R_S$ to be monotonically increasing with the current $I_{sd}$ flowing across the device. This assumption was motivated by the need to account for nonlinearities in the series resistance coming primarily from the source/drain contacts to the two-dimensional hole gas. At $V_{sd} = 0$, $R_S$ is a constant all over the spanned $V_{sg}$ range. At finite $V_{sd}$, $R_S$ varies with $V_{sg}$ due to the $V_{sg}$ dependence of $G$. As a result, the corrected $V_{ds}$ range tends to decrease when lowering $V_{sg}$, and hence increasing $G$.

conduction in the Ge QW (this voltage is sensitive to variations in the static charges on the sample surface).

Figure 3a–c shows the $B$-evolution of the trans-conductance $dG/dV_{sg}$ as a function of $V_{sg}$ with $\vec{B}$ applied along $x$, $y$, and $z$, respectively. The data refer to device D1. In these color maps, the blue regions, where $dG/dV_{sg}$ is largely suppressed, correspond to the plateaus of quantized conductance. On the other hand, the red ridges of enhanced $dG/dV_{sg}$ correspond to the conductance steps between consecutive plateaus, which occur every time the edge of a 1D subband crosses the Fermi energy of the leads. At finite $B$, the red ridges split, following the emergence of new conductance plateaus at odd-integer multiples of $e^2/h$. Upon increasing $B$, the splitting in $V_{sg}$ increases proportionally to the Zeeman energy $E_{Z,n} = |E_{n,\uparrow} - E_{n,\downarrow}|$, where $E_{n,\sigma}$ is the energy of the 1D subband with spin polarization $\sigma$ and orbital index $n$.

For an in-plane $B$, either along $x$ or $y$, the splitting becomes clearly visible only above approximately 2 T. As a result, the explored $B$ range extends up to 6 T. For a perpendicular field, the Zeeman splitting is clearly more pronounced being visible already around 0.2 T. This apparent discrepancy reveals a pronounced $g$-factor anisotropy, with a $g$-factor along the $z$-axis, $g_z$, much larger than the in-plane $g$-factors, $g_x$ and $g_y$. Such a strong anisotropy is expected in the case of two-dimensional hole states with dominant HH character, corroborating the hypothesis of a dominant confinement in the $z$ direction, which is imposed by the QW heterostructure.

Besides causing the Zeeman splitting of the 1D subbands, the applied $\vec{B}$ has an effect on the orbital degree freedom of the hole states. The effect is relatively weak in the case of an in-plane $B$ because the magnetic length, inversely proportional to $\sqrt{B}$, gets as small as the QW thickness only for the highest $B$ values spanned in Figure 3a,b. On the contrary, the relatively weak lateral confinement imposed by the side gates leaves room for a pronounced $B$-induced orbital shift. This manifests in Figure 3c as an apparent bending of the $dG/dV_{sg}$ ridges toward more negative gate voltages.

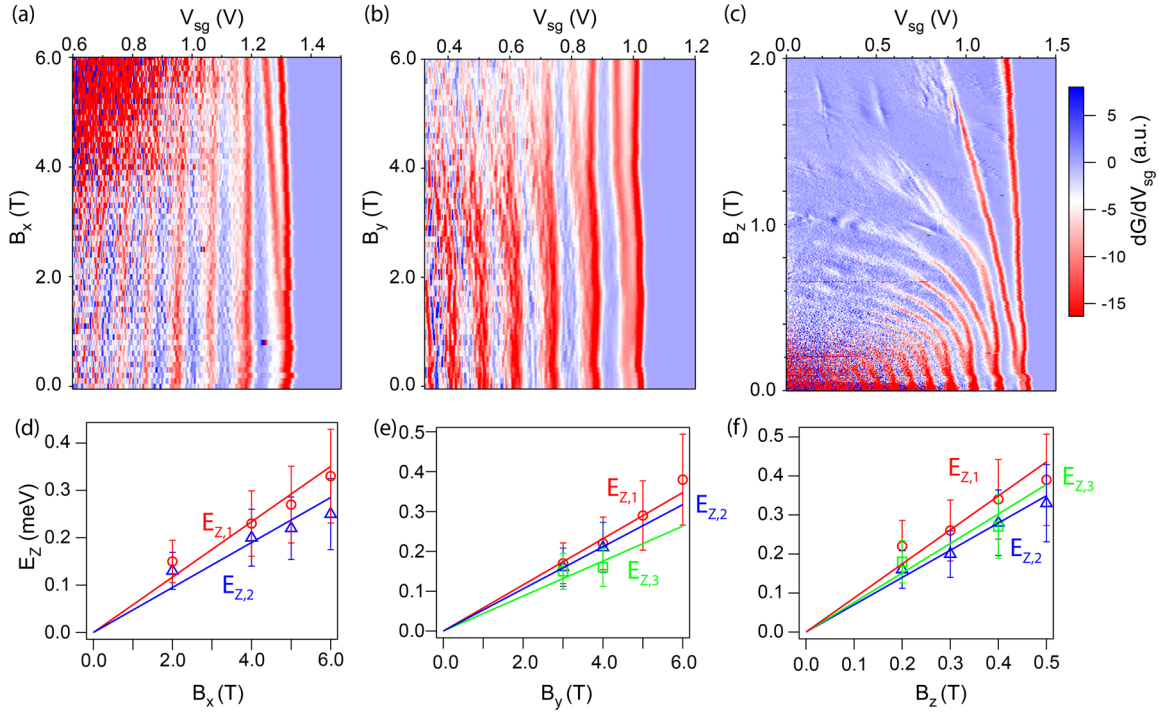


**Figure 3.** (a–c) Numerical derivative of $G$ with respect to $V_{sg}$ as a function of $V_{sg}$ and magnetic field applied along the $x$ (a), $y$ (b), and $z$ (c) directions (data from device D1). (d–f) Zeeman splittings $E_{Z,n} = |E_{n,\uparrow} - E_{n,\downarrow}|$ as a function of magnetic field along the $x$ (d), $y$ (e), and $z$ (f) directions. Red, blue, and green open symbols correspond to the first, second, and third spin-split subbands, respectively. The $g$-factors for each subband are obtained from the slope of the linear fits to the Zeeman relation $E_{Z,n}(B)$ (solid lines). The results are given in Table 1.



DOI: 10.1021/acs.nanolett.8b01457
*Nano Lett.* 2018, 18, 4861–4865

In order to quantitatively estimate the observed Zeeman splittings, and the corresponding $g$-factors, we performed bias-spectroscopy measurements of $dG/dV_{sg}$ as a function of $V_{ds}$ and $V_{sg}$ at different magnetic fields. In these measurements, the $dG/dV_{sg}$ ridges form diamond-shape structures from which we extract the Zeeman energies, as well as the lever-arm parameters relating $V_{sg}$ variations to energy variations. Representative $dG/dV_{sg}(V_{ds},V_{sg})$ measurements and a description of the well-known procedure for the data analysis are given in Supporting Information. Interestingly, for a given $B$, both the Zeeman energy and the lever-arm parameter can vary appreciably from subband to subband.

Figure 3d–f presents the estimated $E_{Z,n}$ values as a function of $B$ for the first few subbands and for the three $B$ directions. Linear fitting to $E_{Z,n} = g_n\mu_B B$ yields the Landé $g$-factors, $g_{x,n}$, $g_{y,n}$, and $g_{z,n}$ for the three perpendicular directions. The extracted $g$-factors for the device D1 are listed in Table 1. We have included also the $g_{z,n}$ values obtained from another device (D3) with $L_g$ = 100 nm.

**Table 1. Summary of Results of $g$-factor Measurements on Device D1 and D3**[a]

| | | $g_1$ | $g_2$ | $g_3$ |
|---|---|---|---|---|
| D1 | $B_x$ | 1.00 ± 0.15 | 0.82 ± 0.12 | |
| | $B_y$ | 1.00 ± 0.15 | 0.91 ± 0.19 | 0.76 ± 0.16 |
| | $B_z$ | 15.0 ± 2.3 | 12.0 ± 1.8 | 13.0 ± 2.8 |
| D3 | $B_z$ | 12.7 ± 2.2 | 11.8 ± 1.8 | 10.4 ± 1.6 |

[a]These $g$-factors are obtained from the slope of the linear fits in Figure 3d–f and Figure S3c in Supporting Information.

For device D1 (D3), the perpendicular $g$-factor ranges between 12.0 (10.4) and 15.0 (12.7), while the in-plane one is much smaller, varying between 0.76 and 1.00 with no significant difference between $x$ and $y$ directions. A large in-plane/out-of-plane anisotropy in the $g$-factors is consistent with the hypothesis of a dominant HH character. In fact, in the limit of vanishing thickness, the lowest subbands of a Ge QW should approach pure HHs with $g_x \approx g_y \approx 0$ and $g_z = 6\kappa + 27q/2 = 21.27$, where $\kappa$ and $q$ are the Luttinger parameters ($\kappa$ = 3.41 and $q$ = 0.06 for Ge).

In the investigated SiGe QW heterostructure, the HH nature of the first 2D subbands is enhanced by the presence of a biaxial compressive strain in the Ge QW, increasing by ∼40 meV the energy splitting with the first light-hole (LH) subbands.[46] The creation of a 1D constriction does not introduce a significant HH–LH mixing because confinement remains dominated by the QW along the growth axis ($z$). From a measured energy spacing of around 0.65 meV between the first and the second 1D subband (see Supporting Information), we estimate that the hole wave functions of the first subband have a lateral width (along $y$) of approximately 80 nm, which is an order of magnitude larger than the wave function extension along $z$.

The results summarized in Table 1 suggest a slight tendency of the $g$-factors to decrease with the subband index. This trend is consistent with the results of earlier experiments with both electron[39,47] and hole[48−50] quantum point contacts. A possible explanation is that the exchange interaction increases the $g$-factor in the low-density limit.[34,51] Yet hole $g$-factors in quantum point contacts depend also on a complex interplay of spin–orbit coupling, applied magnetic field, and electrostatic potential landscape.[52,53] Acquiring a deep understanding of the $g$-factors reported here would require more extensive and sophisticated experiments together with a nontrivial theoretical analysis, which goes well beyond the scope of the present work.

In conclusion, we have demonstrated ballistic hole transports in 1D quantum wires gate-defined in a $Ge/Si_{0.2}Ge_{0.8}$ heterostructure. The ballistic regime is observed for wires up to 600 nm long. Conductance quantization is observed in channels up to 600 nm long. By investigating the Zeeman splitting of the quantized conductance steps we find that out-of-plane $g$-factors are an order of magnitude larger than the in-plane ones, denoting a pronounced HH character. This can be ascribed to the dominant confinement along the growth axis and to the compressive biaxial strain in the Ge QW. The observation of ballistic 1D hole transport in remarkably long channels and large out-of-plane $g$-factors holds special promise for the development of devices with spin-related functionality. In principle, the fabrication of these devices could be implemented in an industry-standard fab line with the possibility of monolithic integration with conventional silicon electronics.

## ■ ASSOCIATED CONTENT

### Supporting Information

The Supporting Information is available free of charge on the ACS Publications website at DOI: 10.1021/acs.nanolett.8b01457.

Additional experimental data from a gated Hall-bar device, providing information on the transport properties of the two-dimensional hole gas. Additional data from another 1D-wire device (D3). Description of the procedure to extract energy spacings in a 1D channel (PDF)

## ■ AUTHOR INFORMATION


### Corresponding Authors

*E-mail: silvano.defranceschi@cea.fr.

*E-mail: M.Myronov@warwick.ac.uk.

### ORCID

R. Mizokuchi: 0000-0002-0538-271X

M. Myronov: 0000-0001-7757-2187


### Notes

The authors declare no competing financial interest.

## ■ ACKNOWLEDGMENTS

We acknowledge financial support from the Agence Nationale de la Recherche, through the TOPONANO project.

## ■ REFERENCES


(1) Awschalom, D. D.; Flatté, M. E. *Nat. Phys.* **2007**, *3*, 153.

(2) Nadj-Perge, S.; Pribiag, V. S.; van den Berg, J. W. G.; Zuo, K.; Plissard, S. R.; Bakkers, E. P. A. M.; Frolov, S. M.; Kouwenhoven, L. P. *Phys. Rev. Lett.* **2012**, *108*, 166801.

(3) Pribiag, V. S.; Nadj-Perge, S.; Frolov, S. M.; van den Berg, J. W. G.; van Weperen, I.; Plissard, S. R.; Bakkers, E. P. A. M.; Kouwenhoven, L. P. *Nat. Nanotechnol.* **2013**, *8*, 170.

(4) Gerardot, B. D.; Brunner, D.; Dalgarno, P. A.; Öhberg, P.; Seidl, S.; Kroner, M.; Karrai, K.; Stoltz, N. G.; Petroff, P. M.; Warburton, R. J. *Nature* **2008**, *451*, 441.

(5) Bulaev, D. V.; Loss, D. *Phys. Rev. Lett.* **2007**, *98*, 097202.

(6) Fischer, J.; Coish, W. A.; Bulaev, D. V.; Loss, D. *Phys. Rev. B: Condens. Matter Mater. Phys.* **2008**, *78*, 155329.




DOI: 10.1021/acs.nanolett.8b01457
*Nano Lett.* 2018, 18, 4861–4865

(7) Maurand, R.; Jehl, X.; Kotekar-Patil, D.; Corna, A.; Bohuslavskyi, H.; Laviéville, R.; Hutin, L.; Barraud, S.; Vinet, M.; Sanquer, M.; De Franceschi, S. *Nat. Commun.* **2016**, *7*, 13575.
(8) Ono, K.; Giavaras, G.; Tanamoto, T.; Ohguro, T.; Hu, X.; Nori, F. *Phys. Rev. Lett.* **2017**, *119*, 156802.
(9) Watzinger, H.; Kukučka, J.; Vukušić, L.; Gao, F.; Wang, T.; Schäffler, F.; Zhang, J.-J.; Katsaros, G. 2018, arXiv preprint arXiv:1802.00395, accessed on March 18, 2018.
(10) De Franceschi, S.; Kouwenhoven, L.; Schönenberger, C.; Wernsdorfer, W. *Nat. Nanotechnol.* **2010**, *5*, 703.
(11) Clark, T. D.; Prance, R. J.; Grassie, A. D. C. *J. Appl. Phys.* **1980**, *51*, 2736−2743.
(12) de Lange, G.; van Heck, B.; Bruno, A.; van Woerkom, D. J.; Geresdi, A.; Plissard, S. R.; Bakkers, E. P. A. M.; Akhmerov, A. R.; DiCarlo, L. *Phys. Rev. Lett.* **2015**, *115*, 127002.
(13) Casparis, L.; Larsen, T. W.; Olsen, M. S.; Kuemmeth, F.; Krogstrup, P.; Nygård, J.; Petersson, K. D.; Marcus, C. M. *Phys. Rev. Lett.* **2016**, *116*, 150505.
(14) Lutchyn, R.; Bakkers, E.; Kouwenhoven, L.; Krogstrup, P.; Marcus, C.; Oreg, Y. *Nat. Rev. Mater.* **2018**, *3*, 52.
(15) Maier, F.; Klinovaja, J.; Loss, D. *Phys. Rev. B: Condens. Matter Mater. Phys.* **2014**, *90*, 195421.
(16) Lu, W.; Xiang, J.; Timko, B. P.; Wu, Y.; Lieber, C. M. *Proc. Natl. Acad. Sci. U. S. A.* **2005**, *102*, 10046−10051.
(17) Kotekar-Patil, D.; Nguyen, B.-M.; Yoo, J.; Dayeh, S. A.; Frolov, S. M. *Nanotechnology* **2017**, *28*, 385204.
(18) Xiang, J.; Vidan, A.; Tinkham, M.; Westervelt, R. M.; Lieber, C. M. *Nat. Nanotechnol.* **2006**, *1*, 208−213.
(19) Su, Z.; Zarassi, A.; Nguyen, B.-M.; Yoo, J.; Dayeh, S. A.; Frolov, S. M. 2016, arXiv preprint arXiv:1610.03010, accessed March 18, 2018.
(20) Katsaros, G.; Golovach, V. N.; Spathis, P.; Ares, N.; Stoffel, M.; Fournel, F.; Schmidt, O. G.; Glazman, L. I.; De Franceschi, S. *Phys. Rev. Lett.* **2011**, *107*, 246601.
(21) Ares, N.; Katsaros, G.; Golovach, V. N.; Zhang, J. J.; Prager, A.; Glazman, L. I.; Schmidt, O. G.; Franceschi, S. D. *Appl. Phys. Lett.* **2013**, *103*, 263113.
(22) Zhang, J. J.; Katsaros, G.; Montalenti, F.; Scopece, D.; Rezaev, R. O.; Mickel, C.; Rellinghaus, B.; Miglio, L.; De Franceschi, S.; Rastelli, A.; Schmidt, O. G. *Phys. Rev. Lett.* **2012**, *109*, 085502.
(23) Myronov, M.; Morrison, C.; Halpin, J.; Rhead, S.; Casteleiro, C.; Foronda, J.; Shah, V. A.; Leadley, D. *Jpn. J. Appl. Phys.* **2014**, *53*, 04EH02.
(24) Shi, Q.; Zudov, M. A.; Morrison, C.; Myronov, M. *Phys. Rev. B: Condens. Matter Mater. Phys.* **2015**, *91*, 241303.
(25) Laroche, D.; Huang, S.-H.; Chuang, Y.; Li, J.-Y.; Liu, C.; Lu, T. *Appl. Phys. Lett.* **2016**, *108*, 233504.
(26) Gul, Y.; Holmes, S. N.; Newton, P. J.; Ellis, D. J. P.; Morrison, C.; Pepper, M.; Barnes, C. H. W.; Myronov, M. *Appl. Phys. Lett.* **2017**, *111*, 233512.
(27) Gul, Y.; Holmes, S. N.; Myronov, M.; Kumar, S.; Pepper, M. *J. Phys.: Condens. Matter* **2018**, *30*, 09LT01.
(28) Hendrickx, N.; Franke, D.; Sammak, A.; Kouwenhoven, M.; Sabbagh, D.; Yeoh, L.; Li, R.; Tagliaferri, M.; Virgilio, M.; Capellini, G. 2018, arXiv preprint arXiv:1801.08869, accessed February 11, 2018.
(29) With an expected Ge/SiGe valence-band offset of 150 meV, a quantum well thickness of 22 nm results in a prominent size quantization leading to the formation of two-dimensional subbands with well-separated energies (energy spacing of 10−20 meV). At the same time, a thickness of 22 nm is large enough to ensure a strong confinement of the heavy-hole ground-state subband, which remains close to the valence band edge.
(30) Myronov, M.; Morrison, C.; Halpin, J.; Rhead, S.; Casteleiro, C.; Foronda, J.; Shah, V. A.; Leadley, D. *Jpn. J. Appl. Phys.* **2014**, *53*, 04EH02.
(31) This is done to prevent gate leakage caused by threading dislocations produced during the wedge bonding of the gate pads (which are positioned around the mesa structure).
(32) Büttiker, M. *Phys. Rev. B: Condens. Matter Mater. Phys.* **1990**, *41*, 7906−7909.
(33) van Wees, B. J.; van Houten, H.; Beenakker, C. W. J.; Williamson, J. G.; Kouwenhoven, L. P.; van der Marel, D.; Foxon, C. T. *Phys. Rev. Lett.* **1988**, *60*, 848−850.
(34) Thomas, K. J.; Nicholls, J. T.; Simmons, M. Y.; Pepper, M.; Mace, D. R.; Ritchie, D. A. *Phys. Rev. Lett.* **1996**, *77*, 135−138.
(35) Kristensen, A.; Bruus, H.; Hansen, A. E.; Jensen, J. B.; Lindelof, P. E.; Marckmann, C. J.; Nygård, J.; Sørensen, C. B.; Beuscher, F.; Forchel, A.; Michel, M. *Phys. Rev. B: Condens. Matter Mater. Phys.* **2000**, *62*, 10950−10957.
(36) Cronenwett, S. M.; Lynch, H. J.; Goldhaber-Gordon, D.; Kouwenhoven, L. P.; Marcus, C. M.; Hirose, K.; Wingreen, N. S.; Umansky, V. *Phys. Rev. Lett.* **2002**, *88*, 226805.
(37) Danneau, R.; Klochan, O.; Clarke, W. R.; Ho, L. H.; Micolich, A. P.; Simmons, M. Y.; Hamilton, A. R.; Pepper, M.; Ritchie, D. A. *Phys. Rev. Lett.* **2008**, *100*, 016403.
(38) Komijani, Y.; Csontos, M.; Ihn, T.; Ensslin, K.; Meir, Y.; Reuter, D.; Wieck, A. D. *Phys. Rev. B: Condens. Matter Mater. Phys.* **2013**, *87*, 245406.
(39) Heedt, S.; Prost, W.; Schubert, J.; Grützmacher, D.; SchäPers, T. *Nano Lett.* **2016**, *16*, 3116−3123.
(40) Saldaña, J.; Žitko, R.; Cleuziou, J.; Lee, E.; Zannier, V.; Ercolani, D.; Sorba, L.; Aguado, R.; De Franceschi, S. 2018, arXiv preprint arXiv:1801.01855, accessed on March 18, 2018.
(41) Micolich, A. P.; Zülicke, U. *J. Phys.: Condens. Matter* **2011**, *23*, 362201.
(42) Iqbal, M. J.; Levy, R.; Koop, E. J.; Dekker, J. B.; de Jong, J. P.; van der Velde, J. H. M.; Reuter, D.; Wieck, A. D.; Aguado, R.; Meir, Y.; van der Wal, C. H. *Nature* **2013**, *501*, 79.
(43) Bauer, F.; Heyder, J.; Schubert, E.; Borowsky, D.; Taubert, D.; Bruognolo, B.; Schuh, D.; Wegscheider, W.; von Delft, J.; Ludwig, S. *Nature* **2013**, *501*, 73.
(44) Brun, B.; Martins, F.; Faniel, S.; Hackens, B.; Bachelier, G.; Cavanna, A.; Ulysse, C.; Ouerghi, A.; Gennser, U.; Mailly, D.; Huant, S.; Bayot, V.; Sanquer, M.; Sellier, H. *Nat. Commun.* **2014**, *5*, 4290.
(45) Iagallo, A.; Paradiso, N.; Roddaro, S.; Reichl, C.; Wegscheider, W.; Biasiol, G.; Sorba, L.; Beltram, F.; Heun, S. *Nano Res.* **2015**, *8*, 948−956.
(46) Failla, M.; Myronov, M.; Morrison, C.; Leadley, D. R.; Lloyd-Hughes, J. *Phys. Rev. B: Condens. Matter Mater. Phys.* **2015**, *92*, 045303.
(47) Martin, T. P.; Szorkovszky, A.; Micolich, A. P.; Hamilton, A. R.; Marlow, C. A.; Linke, H.; Taylor, R. P.; Samuelson, L. *Appl. Phys. Lett.* **2008**, *93*, 012105.
(48) Daneshvar, A. J.; Ford, C. J. B.; Hamilton, A. R.; Simmons, M. Y.; Pepper, M.; Ritchie, D. A. *Phys. Rev. B: Condens. Matter Mater. Phys.* **1997**, *55*, R13409−R13412.
(49) Danneau, R.; Klochan, O.; Clarke, W. R.; Ho, L. H.; Micolich, A. P.; Simmons, M. Y.; Hamilton, A. R.; Pepper, M.; Ritchie, D. A.; Zülicke, U. *Phys. Rev. Lett.* **2006**, *97*, 026403.
(50) Srinivasan, A.; Hudson, K. L.; Miserev, D.; Yeoh, L. A.; Klochan, O.; Muraki, K.; Hirayama, Y.; Sushkov, O. P.; Hamilton, A. R. *Phys. Rev. B: Condens. Matter Mater. Phys.* **2016**, *94*, 041406.
(51) Wang, C.-K.; Berggren, K.-F. *Phys. Rev. B: Condens. Matter Mater. Phys.* **1996**, *54*, R14257−R14260.
(52) Miserev, D. S.; Sushkov, O. P. *Phys. Rev. B: Condens. Matter Mater. Phys.* **2017**, *95*, 085431.
(53) Miserev, D. S.; Srinivasan, A.; Tkachenko, O. A.; Tkachenko, V. A.; Farrer, I.; Ritchie, D. A.; Hamilton, A. R.; Sushkov, O. P. *Phys. Rev. Lett.* **2017**, *119*, 116803.



DOI: 10.1021/acs.nanolett.8b01457
*Nano Lett.* 2018, 18, 4861−4865